TITLE

Glycosomal Bromodomain Factor 1 from *Trypanosoma cruzi* enhances trypomastigotes cell infection and intracellular amastigotes growth

AUTHORS

Carla Ritagliati[1], Gabriela Vanina Villanova[1,2], Victoria Lucia Alonso[2], Aline Araujo Zuma[3], Pamela Cribb[1,2], María Cristina Machado Motta[3] and Esteban Carlos Serra[1,2]

ADRESSES

[1]Instituto de Biología Molecular y Celular de Rosario (IBR), CONICET. Rosario, Argentina.
[2]Facultad de Ciencias Bioquímicas y Farmacéuticas, Universidad Nacional de Rosario (UNR). Rosario, Argentina.
[3]Instituto de Biofísica Carlos Chagas Filho, Universidade Federal do Rio de Janeiro. Rio de Janeiro, Brazil.
*Corresponding author serra@ibr-conicet.gov.ar

ABSTRACT

Acetylation is a ubiquitous protein modification present in prokaryotic and eukaryotic cells that participates in the regulation of many cellular processes. The bromodomain is the only domain known to bind acetylated lysines. In the last years many bromodomain inhibitors have been developed in order to treat diseases caused by aberrant acetylation of lysine residues and have been tested as anti-parasitic drugs. Here, we report the first characterization of *T. cruzi* Bromodomain Factor 1. *Tc*BDF1 is expressed in all life cycle stages but it is developmentally regulated. It localizes in the glycosomes directed by a PTS2 sequence. The overexpression of *Tc*BDF1 wild type is detrimental for epimastigotes, but it enhances the infectivity rate of trypomastigotes and the replication of amastigotes. On the other hand, the overexpression of a mutated version of *Tc*BDF1 has no effect on epimastigotes, but it does negatively affect on trypomastigotes' infection and amastigotes' replication.

SUMMARY STATEMENT

We characterized Bromodomain Factor 1 from *Trypanosoma cruzi,* a developmentally regulated protein that localizes in the glycosomes of epimastigotes. The overexpression of *Tc*BDF1 wild type is detrimental for epimastigotes but favours trypomastigotes infection, while mutant *Tc*BDF1 diminishes the infectivity rate.

SHORT TITLE

Trypanosoma cruzi Bromodomain Factor 1

KEYWORDS

TRYPANOSOMA; BROMODOMAIN; ACETYLATION; GLYCOSOME

INTRODUCTION

Lysine acetylation is a reversible and highly regulated posttranslational modification that is known to play a key role in regulating transcription and other DNA-dependent nuclear processes (1). Recently, advancement in mass spectrometry allowed characterization of the acetylomes in bacteria (2-10), yeast (11), the protozoan parasites *Toxoplasma gondii* (12) and *Plasmodium falciparum* (13), plants (14), *Drosophila melanogaster* (15), rat (16), and human cells (1, 17-18). These acetylomes consisted of hundreds to thousands of acetylated proteins distributed among the different cellular compartments and involved in several processes such as: transcription, translation, cellular cycle progression, apoptosis, stress response and metabolism. One of the most surprising findings has been that metabolic enzymes are highly represented among the acetylomes. This suggested that changes in acetylation status might alter enzymatic activity to allow the cell to respond to changes in metabolic demands by adjusting flux through critical nodes in the relevant pathways (19). Furthermore, the effects of acetylation appear to be coordinated to simultaneously shunt metabolic flux down specific pathways and away from others. These efforts have uncovered a stunning complexity of the acetylome that potentially rivals that of the phosphoproteome. The remarkably ubiquitous and conserved nature of protein acetylation revealed by these studies suggests the regulatory power of this dynamic modification.

The bromodomain is the only known protein domain involved in the recognition of acetylated lysines. It represents an evolutionarily conserved module, present mostly in nuclear proteins. It has an atypical left-handed four-helix bundle connected by two loops that form the surface accessible hydrophobic pocket where the acetyl-lysine binding site is located. Bromodomains are present in many transcription factors and chromatin regulators, also they can interact with other proteins in an acetylation-dependent manner and form multisubunit complexes (20). We have previously described in *Trypanosoma cruzi* a nuclear bromodomain (*Tc*BDF2), which binds H4K10 and H4K14 (21); and a cytoplasmic bromodomain (*Tc*BDF3), which interacts with acetylated a-tubulin (22).

The trypanosomatid parasites *Leishmania* spp., *Trypanosoma brucei* and *Trypanosoma cruzi* (also known as "TriTryps") are a group of early divergent flagellated protozoa that cause severe diseases in humans including leishmaniasis, sleeping sickness and Chagas disease. They constitute important public health problems in developing countries due to the lack of vaccines and modern therapies (http://www.who.int/). The glycosome is a peroxisome-like organelle specific to trypanosomatids. It contains the first six or seven glycolytic enzymes together with some auxiliary pathways apparently involved in the reoxidation of NADH and in the regeneration of the ATP consumed in the activation of the glucose molecule (23-24). In addition, the glycosome may harbor other enzymatic systems such as: fatty acid β-oxidation (25), sterol synthesis (26-27) and isoprenoids synthesis, among others.

Genes of glycosomal and peroxisomal proteins are encoded in the nucleus necessitating organellar protein import in a posttranslational fashion. This import requires a routing signal. Two main topogenic signals (peroxisome-targeting signal or PTS) that direct the matrix proteins have been described and are well conserved between species. Most of these proteins use a PTS1, a tripeptide motif present at their C-terminus, which is recognized by cytosolic peroxisome-import receptor called peroxin 5 (PEX5). The general consensus sequence of PTS1 is [SAC]-[KRH]-[LM]. The PTS2 consensus sequence, M-$x_{0,20}$-[RK]-[LVI]-x_5-[HKQR]-[LAIVFY], is a nonapeptide that resides near the N-terminus (28), and it is recognized by PEX7. Other proteins are imported upon recognition of a polypeptide-internal signal (I-PTS) (29).

Here, we describe the characterization of Bromodomain Factor 1 from *Trypanosoma cruzi* (*Tc*BDF1), one of the few bromodomain-containing proteins reported outside the nucleus. *Tc*BDF1 is expressed in all life cycle stages but it is developmentally regulated, being more abundant in the infective form (trypomastigotes) than in the replicative forms (epimastigotes and amastigotes). *Tc*BDF1 localizes in the glycosomes and it possesses a PTS2 responsible of its import. The overexpression of *Tc*BDF1 wild type is deleterious for epimastigotes growth and *in vitro* differentiation to metacyclic trypomastigotes, however it increases trypomastigotes infection of Vero cells and amastigotes duplication. On the other hand, when we overexpress a mutant version of *Tc*BDF1, the infectivity of trypomastigotes decreases, but it causes no alteration to epimastigotes replication.

MATERIALS AND METHODS

Parasites.

T. cruzi epimastigote forms (Cl Brener) were cultured at 28°C in liver infusion tryptose (LIT) medium (5 g/L liver infusion, 5 g/L bacto-tryptose, 68 mM NaCl, 5.3 mM KCl, 22 mM Na_2HPO_4, 0.2% (w/v) glucose and 0.002% (w/v) hemin) supplemented with 10% (v/v) heat-inactivated FCS, 100 U/ml penicillin and 100 mg/l streptomycin. Cell viability was assessed by direct microscopic examination.

Cell culture and infections.

Vero cells were cultured in DMEM medium (Life Technologies), supplemented with 2 mM L-glutamine, 10% FCS, 100 U/ml penicillin and 100 μg/ml streptomycin.

Metacyclic trypomastigotes were obtained by spontaneous differentiation of epimastigotes at 28°C. Cell-derived trypomastigotes were obtained by infection with metacyclic trypomastigotes of Vero cell monolayers. After two rounds of infections, the cell-derived trypomastigotes were used for the infection and intracellular amastigotes proliferation experiments. Trypomastigotes were collected by centrifugation of the supernatant of previously infected cultures at 2,000 x g at room temperature for 10 minutes and incubated for 3 hours at 37°C in order to allow the trypomastigotes to move from the pellet into the supernatant. After this period, the supernatant was collected and trypomastigotes were counted in a Neubauer chamber. The purified

trypomastigotes were pre-incubated in the presence or absence of 0.25 µg/ml Tetracycline for 3 hours and then used to infect new monolayers of Vero cells at a ratio of 20 parasites per cell in DMEM supplemented with 2% FCS. After 16 h of infection at 37°C, the free trypomastigotes were removed by successive washes with PBS. Cultures were incubated in complete medium with or without tetracycline (0.25 µg/ml) for 3 days post-infection. Cells were then fixed in methanol and the percentage of infected cells and the mean number of amastigotes per infected cell were determined by counting the slides after Giemsa staining using a Nikon Eclipse Ni-U microscope, by counting ~1000 cells per slide. The significances of the results were analyzed by a two-way ANOVA using GraphPad Prism version 6.0 for Mac. Results are expressed as means ± SEM of triplicates, and represent one of three independent experiments performed.

Cloning and expression of *Tc*BDF1.

DNA purified from *T. cruzi* CL Brener strain was used as a template for PCR with oligonucleotides: BDF1BamHIFw (5'AAGGATCCATGACTGATTTTGTCTCTC'3) and BDF1**HA**XhoIRv (5'AACTCGAG**AGCATAATCCGGCACATCATACGGATA**ATCTCTTCTTCCTCCTCA 3´) using a proofreading polymerase. PCR product was inserted into a pCR®2.1-TOPO® vector (Invitrogen) and sequenced (Maine University facility). The *Tc*BDF1 coding region was introduced into a pENTR3C vector (Gateway® system Invitrogen) using the BamHI/XhoI restriction sites included in the oligonucleotides (underlined). It was then transferred to a destination vector pDEST17 (Gateway® system Invitrogen) by recombination using LR Clonase (Invitrogen) to express *Tc*BDF1 as a His-tag fusion protein. This vector was transformed into *Escherichia coli* BL21 pLysS, and recombinant protein was obtained by expression-induction with 1 mM isopropyl b-D-1-thiogalactopyranoside (IPTG), for 10 h at 37 °C. The protein was purified under denatured conditions by affinity chromatography using Ni–NTA agarose (Qiagen) following the manufacturer's instructions.

The double mutant (*Tc*BDF1-Y102A/V109A) was constructed using a PCR-based site directed-mutagenesis strategy with the following oligonucleotides: BDF1YxAFw (5´GCTACGCGGCCAATGGTGAAG'3), BDF1YxARv (5´CTTCACCATTGGCCGCGTAGC'3), BDF1VxAFw (5´GTTTCTCCAGCGGCAGCGTTG'3) and BDF1VxARv (5´CAACGCTGCCGCTGGAGAAAC'3). Both resulting PCR products obtained were used simultaneously as templates in a new PCR with BDF1BamHIFw and BDF1HAXhoIRv. The *Tc*BDF1 double mutant coding region was inserted into a pCR®2.1-TOPO® vector (Invitrogen), sequenced (Maine University facility) and introduced into a pENTR3C vector (Gateway® system Invitrogen) using the BamHI/XhoI restriction sites included in the oligonucleotides (underlined). *Tc*BDF1 wild type (*Tc*BDF1wt) and *Tc*BDF1 double mutant (*Tc*BDF1dm) coding regions were transferred from pENTR3C vector to p*Tc*INDEX-GW (Alonso, Ritagliati et al., 2014) by recombination using LR clonase II enzyme mix (Invitrogen).

***Tc*BDF1 fusion constructs.**

DNA purified from *T. cruzi* CL Brener strain was used as a template for PCR to amplify *Tc*BDF1 with the oligonucleotides BDF1XbaIFw (5'AATCTAGAATGACTGATTTTGTCTCTC'3) and

BDF1SalIRv (5'AAGTCGACAATCTCTTCTTCCTCCTC´3), TcBDF1ΔN with BDF1ΔNXbaIFw (5'AATCTAGAATGAATTCCTTCTACCGTGAGTG'3) and BDF1SalIRv, and TcBDF1PTS-2 with BDF1XbaIFw and BDF1PTS2SalIRv (5´AAGTCGACGAAGGAATTCTCCAAGTG´3) using a proofreading polymerase. PCR products were inserted into a pCR®2.1-TOPO® vector (Invitrogen) and sequenced. The coding regions were introduced into the vector pTREX-mCherry (30) using the XbaI/SalI restriction sites included in the oligonucleotides (underlined).

Polyclonal antibodies.

Rabbit and mouse polyclonal antisera against *Tc*BDF1 were obtained by inoculating subcutaneously the recombinant protein emulsified in Freunds´adjuvant. Formal animal ethics approval was given for this work. Animals were housed and maintained according to institution guidelines. The animals were injected three times with 2 weeks intervals between each dose and bled two weeks after the final injection (31).

Transfection of parasites.

Epimastigote forms of *T. cruzi* CL Brener were grown at 28°C in liver infusion tryptose (LIT) medium, supplemented with 10% fetal calf serum (FCS), to a density of approximately 3×10^7 cells ml^{-1}. Parasites were harvested by centrifugation at 4,000 × g for 5 min at room temperature, washed once in phosphate-buffered saline (PBS) and resuspended in 0.4 ml of electroporation buffer pH 7.5 (140 mM NaCl, 25 mM HEPES, 0.74 mM Na_2HPO_4) to a density of 1×10^8 cells ml^{-1}. Cells were then transferred to a 0.2 cm gap cuvette (Biorad) and ~50 µg of DNA were added. The mixture was placed on ice for 10 min and then subjected to 2 pulses of 450 V and 500 µF using GenePulser II (Bio-Rad, Hercules, USA). After electroporation, cells were transferred into 3 ml of LIT medium containing 10% FCS, where they were incubated at 28°C. After 24 h of incubation, the antibiotic (Hygromycin or Geneticin) was added to an initial concentration of 125 µg ml^{-1}. Then, 72 to 96 hours after electroporation, cultures were diluted 1:10 and antibiotic concentration was doubled. Stable resistant cells were obtained approximately 20 days after transfection. The pTREXmCherry fusion transfectants were selected with Geneticin (G418; Life Technologies).

For inducible expression of *Tc*BDF1 wilt type and double mutant in the parasite, we first generated a cell line expressing T7 RNA polymerase and tetracycline repressor genes by transfecting epimastigotes with the plasmid pLew13. After selection with G418, this parental cell line was then transfected with p*Tc*INDEX-GW constructs and transgenic parasites were obtained after 3 weeks of selection with 100 µg/ml G418 and 200 µg/ml Hygromycin B (Sigma).

***In vitro* metacyclogenesis.**

To quantify the metacyclogenesis rate of the transfected lines, epimastigotes were differentiated *in vitro* following the procedure described by Contreras and coworkers (32) using chemically defined conditions (TAU3AAG medium). Briefly, cells were washed with PBS and incubated in TAU medium (190 mM NaCl, 17 mM KCl, 2 mM $MgCl_2$, 2mM $CaCl_2$, 8 mM phosphate buffer pH 6.0)

in the absence or presence of 0.25 µg/ml Tetracycline, reaching a density of 5 x 10^8 parasites/ml at 28°C for 2 hours. Then they were diluted 1:100 in TAU3AAG Medium (TAU medium plus 10 mM Glucose, 2 mM L-Aspartic Acid, 50 mM L-Glutamic Acid and 10 mM L-Proline) and incubated at 28 °C for 72 hours, again in the absence or presence of Tetracycline. Finally, the parasites were fixed, stained with Giemsa, visualized with a Nikon Eclipse Ni-U microscope and counted using ImageJ software (33). Only parasites with a fully elongated nucleus and a round kinetoplast at the posterior portion end of the parasite were considered metacyclic forms (34). Five hundred parasites from each triplicate were counted and the experiment was repeated tree times.

Trypanosoma cruzi protein extracts.

Exponentially growing epimastigotes were washed twice with cold PBS, pellets were resuspended in urea lysis buffer (8 M Urea, 20 mM Hepes pH 8, 1 mM phenylmethylsulphonyl fluoride (PMSF), and Protease Inhibitor Cocktail set I, Calbiochem), incubated at room temperature for 20 minutes and boiled for 5 minutes with protein loading buffer. Insoluble debris was eliminated by centrifugation. The same procedure was applied to amastigote and trypomastigote cellular pellets.

Nuclear and non-nuclear extracts were prepared from 2 x 10^{10} exponentially growing parasites. After washing, parasites were lysed in hypotonic Buffer A (10 mM HEPES pH 8, 50 mM NaCl, 1 mM EDTA, 5 mM MgCl2, 1% v/v Nonidet P-40, 1 mM phenylmethylsulphonyl fluoride (PMSF), 10 µg ml^{-1} aprotinin, 0.25% Triton X-100), 5% v/v glycerol was added and the pellet was collected by centrifugation. The supernatant corresponded to the non-nuclear fraction. Pellets were washed with Buffer B (10 mM HEPES pH 8, 140 mM NaCl, 1 mM EDTA, 5 mM $MgCl_2$ 5% v/v glycerol, 1 mM PMSF, 10 µg ml^{-1} aprotinin) and incubated for 10 min on ice. Nuclei were collected by centrifugation and resuspended in Buffer C (10 mM HEPES pH 8, 400 mM NaCl, 0.1 mM EDTA, 0.5 mM DTT, 5% v/v glycerol, 1 mM PMSF, 10 µg ml^{-1} aprotinin), incubated for 1 h on ice and sonicated. This extraction was repeated three times and supernatants were precipitated with 20% trichloroacetic acid overnight at 4 °C.

Partial permeabilization by digitonin treatment.

Parasites in exponential phase were collected, washed and suspended in buffer A (20 mM Tris–HCl, pH 7.2 with 225 mM sucrose, 20 mM KCl, 10 mM KH_2PO_4, 5 mM $MgCl_2$, 1 mM Na_2EDTA and 1 mM DTT) at a concentration of 1 mg ml^{-1} protein and fractionated in several tubes. The required amount of digitonin was added to each of these tubes (each tube contained a different digitonin concentration), and the suspensions incubated at 28 °C for 20 min before being centrifuged at 14,000 x g for 2 min at 4 °C. The assayed enzymatic activities were determined in the supernatant and occasionally in the cell pellet in the presence of 0.1% (v/v) Triton X-100 and 150 mM NaCl.

Subcellular fractionation by differential centrifugation.

T. cruzi CL Brener epimastigotes in exponential growth phase were centrifuged for 10 min at 2,000 x g, and washed twice in homogenization buffer (25 mM Tris-HCl pH 8, 1 mM EDTA, 0.25 M

sucrose, 1 mM PMSF). The parasites were grinded in a pre-chilled mortar with 1 x wet weight silicon carbide until no intact cells were observed under the light microscope. The lysate was diluted and centrifuged at 100 x g for 10 min to remove the silicon carbide. Unbroken cells, nuclei and debris were sedimented at 1,000 x g for 10 min (Fraction N). From the resulting soluble extract a large-granule fraction (LG) was separated at 5,000 x g for 15 min, a small-granule fraction (SG) at 20,000 x g for 20 min and microsomal fraction (M) at 139,000 x g for 1 h (35). All the sediments were resuspended in urea lysis buffer.

Western blot analysis.

For Western blots, proteins of the diverse fractions were first separated by polyacrylamide gel electrophoresis in the presence of SDS and transferred to nitrocellulose membrane. Proteins were visualized by Ponceau S staining. Membranes were treated with 10% non-fat milk in PBS for 1 h, and then with specific antibodies diluted in PBS for 3 h. Bound antibodies were detected using peroxidase labeled anti-mouse, anti-rabbit IgGs (GE Healthcare) or anti-rat IgG (Thermo Scientific) and developed using ECL Prime kit (GE Healthcare) according to manufactures protocol.

The fractions obtained with the different subcellular fractionations were analyzed by Western blot with antibodies against *Tc*BDF1 and several markers: anti-Tyrosine aminotransferase, anti-Malate dehydrogenase glycosomal and mitochondrial isoforms, anti-Hexokinase, anti-Bromodomain Factor 2 and anti-Bromodomain Factor 3.

Immunocytolocalization.

The parasites were centrifuged, washed twice in PBS, added to the poly-L-lysine coated slides and then fixed with 4% formaldehyde in PBS at room temperature for 20 min. Fixed parasites were washed with PBS and permeabilized with 0.1% Triton X-100 in PBS for 5 min. After washing with PBS, parasites were incubated with the indicated antibodies diluted in 1% BSA–PBS for 1 h at room temperature. For co-localizations, both antibodies were used at the same time. The antibodies were washed with PBS and the slides incubated with anti-rabbit or anti-mouse IgG antibody fluorescent conjugates. The slides were mounted with VectaShield (Vector Laboratories) in the presence of 2 μg ml^{-1} of DAPI in PBS. Images were acquired in a Nikon Eclipse E300 and a Nikon Eclipse TE-2000-E2 microscopes. The programs Adobe Photoshop CS Version 8.0.1. (Adobe System Incorporated) and Nikon EZ-C1 FreeViewer version 3.70 (Nikon Corporation) were used to analyze the images.

Electron microscopy.

Parasites were washed twice in PBS and fixed in 2.5% glutaraldehyde in 0.1 M cacodylate buffer pH 7.2, for 1 h. Then, cells were washed in 0.1 M cacodylate buffer pH 7.2, and postfixed for 1 h in 1% osmium tetroxide containing 0.8% potassium ferrocyanide, 5 mM $CaCl_2$ in 0.1 M cacodylate buffer. After postfixation, cells were washed in the same buffer, dehydrated in a series of increasing acetone concentrations and embedded in Epon—first as a mixture of Epon and

acetone (1:1) and then as pure Epon. Ultrathin sections were obtained using an Ultracut Reichert Ultramicrotome and mounted on 400-mesh copper grids. Samples were stained with uranyl acetate and lead citrate and then analyzed using a Zeiss 900 transmission electron microscope.

RESULTS

Trypanosoma cruzi bromodomain factor 1 (*Tc*BDF1).

Trypanosoma cruzi CDS TcCLB.506247.80 codes for a 295 amino acids protein with a predicted molecular weight of 33.8 kDa and an isoelectric point of 9.18, which contains a bromodomain (pfam: PF00439) in the N-terminal half of the protein, from F30 to M120. Orthologous genes are present in other trypanosomatids, the *T. brucei* (Tb927.10.8150) and *Leishmania mayor* (LmjF.36.6880) proteins have an identity of 44% and 31% with *Tc*BDF1 respectively (Figure S1A). The C-terminal region does not show similarity with any other sequence present in databases, and it can be divided into a portion rich in glutamines (28.5 % Q) and a portion rich in acidic amino acids, such as aspartic and glutamic acid (21.8% E+D), and serines (10.9% S). In general, these highly charged low complexity sequences are considered prone to participate in protein–protein interaction. In higher eukaryotes, bromodomains are usually found associated to other domains or enzymatic activities in the same polypeptide; however, this is not the situation with *Tc*BDF1, nor with *Tc*BDF2 and *Tc*BDF3.

A multiple alignment of *Tc*BDF1 with other bromodomains (Figure S1B) revealed the typical structure of a four-helix, left-twisted bundle (36). Despite the low similarity among the aligned sequences, the amino acids previously shown to be involved in acetylated-lysine binding are conserved or conservatively substituted.

*Tc*BDF1 three-dimensional structure was predicted by I-TASSER (37) server based on homology with other known bromodomain-containing proteins and as expected, the model with the highest score presents four alfa helixes (αA, αB, αC and αZ) and two loops (ZA and BC) characteristic of bromodomains (Figure S1C). The conserved amino acids important for binding of acetyl lysine are indicated in the figure.

*Tc*BDF1 is differentially expressed throughout the life cycle.

In order to evaluate *Tc*BDF1 expression in *T. cruzi*, antibodies were raised against the recombinant protein and purified by affinity chromatography. After confirming the specificity of the antibodies, they were used in western blots to test *Tc*BDF1 expression in total lysates of epimastigotes, amastigotes and trypomastigotes and in immunofluorescense assays of fixed parasites (Figure 1). Figure 1A shows that the expression of *Tc*BDF1 is developmentally regulated throughout *T. cruzi* life cycle; its expression levels are higher in trypomastigotes than in amastigotes and epimastigotes. As can be seen in Figure 1B, *Tc*BDF1 is localized out of the nucleus in the three developmental stages.

*Tc*BDF1 is a glycosomal protein.

Several approaches were used to determine the localization of *Tc*BDF1 in epimastigotes: three different subcellular fractionation methods followed by western blot (Figure 2) and fluorescense analysis (Figure 3). First, nuclear and non-nuclear extracts were prepared: unlike the nuclear marker, *Tc*BDF2, which was only observed at the nuclear fraction, *Tc*BDF1 was observed at the non-nuclear fraction (Figure 2A). Second, a subcellular fractionation by differential centrifugation was performed: *Tc*BDF1 was present in Fraction M, enriched for glycosomes, as was confirmed using the glycosomal markers glycosomal Malate dehydrogenase (MDHg) and Hexokinase (HK) (Figure 2B). Finally, a progressive permeabilization of epimastigotes was performed in the presence of increasing amounts of digitonin. The fractions obtained at each digitonin concentration were analyzed by western blot with antibodies against *Tc*BDF1 and several markers (Figure 2C). The release of the cytosolic markers, Tyrosine aminotransferase (TAT) and *Tc*BDF3, was complete at about 0.08 mg digitonin mg protein $^{-1}$. At this concentration the glycosomal markers, HK and MDHg, were only partially detected and their release was complete at 0.20-0.24 mg digitonin mg protein $^{-1}$. The mitochondrial marker, mitochondrial Malate dehydrogenase (MDHm), was completely released at about 0.50 mg digitonin mg protein $^{-1}$. *Tc*BDF1 was partially detected at 0.16 mg digitonin mg protein $^{-1}$ and its liberation was complete at 0.28 mg digitonin mg protein $^{-1}$. *Tc*BDF1 pattern was similar to HK and MDHg patterns, both glycosomal proteins. All these results strongly suggest that *Tc*BDF1 is located in the glycosomes.

Furthermore, as can be seen in the immunofluorescense analysis (Figure 3A), *Tc*BDF1 and Hexokinase co-localized in epimastigotes simultaneously stained with the polyclonal mouse anti-*Tc*BDF1 and rabbit anti-*Tc*HK. In order to confirm the glycosomal localization of *Tc*BDF1, epimastigotes were co-transfected with pTEX-GFP-PTS1 and pTREX-*Tc*BDF1-Cherry, and the transient parasites were analyzed by confocal microscopy. As can be observed in Figure 3B, *Tc*BDF1-Cherry co-localized with the GFP protein directed to the glycosomes by the PTS1 importing signal (38).

Identification of *Tc*BDF1 PTS2 signal.

The amino acids sequence of *Tc*BDF1 was analyzed with the PeroxisomeDB server (www.peroxisomedb.org/target_signal.php) and by visual inspection. An alignment of the possible PTS2 present in *Tc*BDF1 N-terminus with known PTS2 sequences is shown in Figure S2. PTS2 is less conserved and found in fewer peroxisomal proteins than PTS1. However, both cytosolic receptors, PEX5 and PEX7, have orthologous in all trypanosomatids.

To determine if the N-terminus of *Tc*BDF1 is responsible for its import to the glycosome, we transiently transfected epimastigotes with constructs coding the whole protein (*Tc*BDF1), a truncated version which lacks the first 27 amino acids (*Tc*BDF1ΔN) or only the N-terminus targeting signal (*Tc*BDF1PTS2), fused to Cherry fluorescent protein. The intracellular localization of the different fusion proteins was determined by confocal microscopy (Figure 4). While *Tc*BDF1-Cherry shows the typical glycosomal granular pattern previously observed by immunofluorescense for *Tc*BDF1 and Hexokinase, *Tc*BDF1ΔN-Cherry is spread throughout the cytoplasm. In the case of *Tc*BDF1PTS2-Cherry, in addition to the punctated pattern, some

cytosolic fluorescence was also detected. The same phenomenon has been described for mammalian cells expressing the minimal PTS2 (39). As discussed by Blattner and coworkers (40), there are three possible explanations for this. One possibility is that the PTS2 sequence does not function well as a consequence of joining to Cherry; probably some conformational effects may be reducing the accessibility of the signal sequence. Secondly, it is possible that two sequences are necessary for import. A third possibility is that we are observing 'overflow' from the glycosomes, because the PTS2 receptors may be saturated.

Inducible expression of wild type and mutant *Tc*BDF1.

In order to assess the function of *Tc*BDF1 in *Trypanosoma cruzi,* parasites expressing wild type and double mutant version of *Tc*BDF1 (here after *Tc*BDF1dmHA) under the control of a Tetracycline-regulated promoter were obtained as described in section 2.6. The double mutant version of *Tc*BDF1 was constructed as described in section 2.3, changing Tyr102 and Val109 for Alanine based on sequence alignments with human PCAF bromodomain (Figure S3). Homologue mutations in *Hs*PCAF were found to disrupt the bromodomain acetyl-lysine binding capacity without altering its structure (41).

Overexpression was performed using the *T. cruzi* inducible vector p*Tc*INDEXGW (42). The induction of the expression by Tetracycline was tested by western blot (Figure 5A and 5B) and immunofluorescense (Figure 5C). Western blot analysis of whole-cell extracts with rat monoclonal anti-HA antibodies revealed the expression of both constructs after the addition of Tetracycline, at their expected molecular weights. No leaky expression was observed in the uninduced parasite lines (Figure 5A). The western blot with the specific antibodies against *Tc*BDF1 shows a high degree of overexpression (~10-fold) in the induced lines (Figure 5B).

***Tc*BDF1 wild type overexpression is deleterious for epimastigotes replication and induces nuclear and glycosomal ultrastructural alterations.**

We monitored the effect of the overexpression on epimastigote growth by counting cell numbers daily after protein induction. Figure 6A shows a replication defect in CL Brener *Tc*BDF1wtHA cell line that lead to growth arrest and death. These epimastigotes exhibit aberrant morphologies with multiple kinetoplasts and flagella (Figure 6B), as was already described for dysfunctional cell cycle parasites (43). When observed by electron microscopy, these induced parasites show nuclear alterations in comparison to uninduced cells (Figure 7A) such as condensation (Figure 7B) followed by dispersion (Figure 7C) of the nucleolus granular region, as well as nucleolar fragmentation (Figure 7E) and nuclear disorganization (Figure 7E). Furthermore, a hyper compactation of the chromatin situated at the nucleus periphery (Figure 7F) was observed and is compatible with an apoptotic process. Induced parasites also exhibit larger glycosomes that are less electrodense (7G-I), this can be related to higher protein levels importation. In contrast, parasites harboring *Tc*BDF1dmHA grew at similar rates in the absence and presence of Tetracycline (Figure 6A) and presented a normal cellular ultrastructure (not shown).

Effect of *Tc*BDF1 overexpression on *in vitro* metacyclogenesis.

In vitro metacyclic trypomastigotes were produced from epimastigotes using TAU medium, in the absence (-Tet) or presence (+Tet) of Tetracycline. *Tc*BDF1dmHA overexpression had no effect on the differentiation to trypomastigotes, whereas *Tc*BDF1wtHA strain showed a meaningful decrease of metacyclogenesis, probably due to its deleterious effect in epimastigotes (Figure 8).

*Tc*BDF1 wild type enhances the infectivity of trypomastigotes.

To study the importance of *Tc*BDF1 expression in trypomastigotes´ infectivity and in the replicative form present inside the mammalian host, we investigated how the transgenic lines induced with Tetracycline performed *in vitro* for invasion and replication in host cells. Trypomastigotes were pre-incubated in the presence or absence of 0.25 µg/ml Tetracycline and then used to infect Vero cells at a ratio of 20 parasites per cell. After 16 h of infection at 37°C, the free trypomastigotes were washed out and replaced by complete medium alone or with Tetracycline (0.25 µg/ml) for 3 days post-infection. Microscopic quantification of Vero cells stained with Giemsa showed that the overexpression of *Tc*BDF1wtHA improved the infective capacity of trypomastigotes [(+/-) vs (-/-)] (Figure 9A) and the replication rate of intracellular amastigotes [(-/+) vs (-/-)] (Figure 9B). In contrast, the overexpression of *Tc*BDF1dmHA diminished the infectivity of trypomastigotes and slightly decreased the proliferation of amastigotes.

DISCUSSION

We present herein the first experimental characterization of *Trypanosoma cruzi* Bromodomain Factor 1. The expression of this protein is developmentally regulated throughout *T. cruzi* life cycle, being more abundant in the infective form than in the replicative forms.

One of the most remarkable features of *Tc*BDF1 is its glycosomal localization. Even though it is not possible to assure that this organelle is the only intracellular compartment where *Tc*BDF1 is located, the experimental data presented supports the idea that most of the protein is placed at the glycosome where it is directed by a PTS2 signal peptide.

The existence of non-nuclear bromodomains is not a novelty in *T. cruzi*. As already mentioned, we recently described a cytoplasmic and flagellar *Tc*BDF3 (22). Some bromodomain-containing proteins from mammals are also found in the cytoplasm, but all the cases reported so far are of nuclear proteins that only localize in the cytoplasm under very particular situations, like ovarian folliculogenesis or spinal cord development (44-46). On the other hand, there has been no bromodomain-containing protein reported to date that localize in an organelle other than the nucleus. As we already proposed, the presence of non-nuclear bromodomains could be another ancient feature of trypanosomatids absent in mammalian host cells.

The presence of a bromodomain factor in the glycosome opens a number of new questions about the existence of acetylation and its function in this organelle. In a preliminary acetylome study of *T. cruzi* epimastigotes performed in our group, 150 acetylated proteins were identified. Thirty percent were enzymes related to metabolic pathways. Among these, five were glycosomal

enzymes belonging to the glucose metabolism, four to the mitochondrial TCA cycle and seven participate in the cell redox homeostasis. These unpublished results are in agreement with those obtained for *T. gondii* (12) and *P. falciparum* (13), and confirm that acetylation is a conserved PTM in protozoans. In addition, the two Sir2 related deacetylases recently characterized in our lab, are cytoplasmic (*Tc*SIR2RP1) and mitochondrial (*Tc*SIR2RP3), and their overexpression impacts in the different stages of *T. cruzi*'s life cycle (47). All these observations support the idea that acetylation is a ubiquous and dynamic PTM in *T. cruzi*, and that acetylomes from different life cycle parasite stages may differ. Taking into account the results already observed in mammals, yeast and bacteria, it seems very plausible that acetylation could also play a role in the metabolic regulation of *T. cruzi*.

It is well established that the different developmental stages of the parasite change their energetic metabolism in response to the available nutrients. Epimastigotes energetic source comes from the oxidation of amino acids, because the concentration of glucose is very low at the gut of the insect. However, in the presence of glucose, epimastigotes rapidly switch to aerobic glucose fermentation. Metacyclic trypomastigotes obtain their energy from proteins and amino acids, while bloodstream trypomastigotes catabolise glucose. Amastigotes consume mostly amino and fatty acids. The glycosome confines most of the glycolytic/gluconeogenic pathway together with enzymes belonging to other metabolic pathways. Turnover of glycosomes by autophagy of redundant ones and biogenesis of a new population of organelles with a different set of metabolic enzymes plays a pivotal role in the efficient adaptation of the glycosomal repertoire to the sudden, major nutritional changes encountered during the transitions in the life cycle (48). A relevant feature of these glycosomal metabolic enzymes is that they lack the regulatory inhibition. For example, hexokinase (HK) and phosphofructokinase (PFK) lack the alosteric regulation present in most cells. Under this condition, the antagonic enzymes PFK and fructose-1,6-biphosphatase (FBPase) coexist in the organelle, but FBPase is kept silent under glycolytic conditions due to an unknown mechanism. It has been proposed that a PTM could be responsible for this phenomenon. The differential phosphorylation status of the glycolytic enzymes from procyclic and bloodstream forms of *T. brucei* has been studied, but these data cannot completely explain so far the regulation of the whole activity within the glycosome (49). It has been already demonstrated in other organisms that changes in the nutrients available to cells, altered the total profile of acetylated metabolic enzymes. And that acetylation/deacetylation of proteins has multiple effects, increasing the activity of some metabolic enzymes while inhibiting the activity of others. For example, aldolase is switched off when acetylated in mammals and plants (14, 16). Phosphoglycerate kinase and glyceraldehyde-3-phosphate dehydrogenase from *Arabidopsis* and glycerol-3-phosphate dehydrogenase and phosphoenolpyruvate carboxykinase (PEPCK1) from mammals, are also inhibited by acetylation (14, 16, 18, 50). However, lysine acetylation does not always lead to enzyme inhibition, in mammals; malate dehydrogenase (MDH) acetylation increases its enzyme activity (18). Furthermore, the effects of acetylation appear to be coordinated to simultaneously shunt metabolic flux down specific pathways and away from others. We consider that acetylation has to be seriously taken into account as an important PTM responsible for the regulation of the

metabolic enzymes in the glycosome. Even though the data available about acetylation in glycolitic enzymes from trypanosomatids is very limited in order to build a hypothesis, it is clear that in most other cells acetylation leads to down regulation of glycolisis.

Currently, it is hard to define how bromodomains take place in this puzzle. In fact, even though plenty of research has been done on bromodomains of yeast and mammals during the last years, their real role remains elusive in most cases. In the nucleus, the association of bromodomains with acetyltransferases led to the proposition of a role in the hyper acetylation of some regions of the chromatin. In this model, the bromodomain-containing proteins or complexes recognize acetylated histones and promote intensive acetylation. Apart from this, no additional function has been yet proposed. *Tc*BDF1 has no other functional domain apart from the bromodomain, but it probably interacts with other proteins through its low complex C-terminus. It is possible that *Tc*BDF1 could have several roles depending on the different proteins with which it interacts in each developmental stage. It is a reader domain, and its function will vary with its interactors and the requirements of the cell. Although the role and targets of *Tc*BDF1 remain to be determined, we now know its expression is tightly regulated throughout the parasite's life cycle and that overexpression in epimastigotes, where it exhibits low expression levels, is detrimental and triggers cell death. On the other hand, it enhances the infectivity of trypomastigotes and the duplication rate of amastigotes. As reported for other trypanosomatids, the glycosomal function, glycolysis in the bloodstream form and gluconeogenesis in intracellular amastigotes, is essential for viability and virulence. This is in agreement with our results. In this context, *Tc*BDF1 could be part of a global regulatory mechanism of the glycosomal activity either by being part of the acetylation/deacetylation complexes, by protecting acetylated lysines from deacetylases, by participating in the biogenesis of the organelle or acting as a chaperone, localizing acetylated proteins to the glycosome. Considering the overexpressing phenotypes obtained, *Tc*BDF1 could be involved in the up-regulation of gluconeogenesis in the replicative forms, which would be detrimental for epimastigotes grown in the presence of glucose, but favourable for amastigotes. On the other hand, in the infective form, it probably enhances glycolysis and ether-lipids synthesis, which depends on glycosomal enzymes. It has been already described that Leishmania and *T. brucei* have high levels of ether-lipids, mainly found in the glycosylphosphatidylinositol-anchored glycolipids and glycoproteins present on the surface of the parasites (51-52), and are important for infection.

The search for inhibitors of lysine acetyltransferases and deacetylases (KATs and KDACs) had a strong impulse in the last years, and the number of diseases associated to alterations in the epigenetic regulation that could be treated with these inhibitors, has significantly increased (53). A number of sirtuin inhibitors have also been assayed against parasites (54). More recently, different families of drugs that target bromodomains from the BET family have shown selective activity in carcinoma models (55). Many other inhibitors of the bromodomain-acetyl lysine interaction have also been developed, putting bromodomains alongside KATs and KDACs as interesting targets for drug development for diseases caused by aberrant acetylation of lysine residues (56). Furthermore, the metabolic disturbance resulting from mislocalization of glycosomal proteins may lead to death of the parasites and for this reason; they are also being

studied with the aim of developing new drugs against parasitic diseases (Barros-Alvarez X et al, 2014). The results presented herein show that *Tc*BDF1 is essential for host invasion and the progression of the infection, and strongly support the idea that bromodomains can be considered as potential targets for the development of new drugs against trypanosomiasis.

ACKNOWLEDGEMENTS

Authors thank Dr. C. Nowiki for the generous gift of anti-*T. cruzi* Tyrosine Amino Transferase and anti-Malate Dehydrogenase (mitochondrial and glycosomal isoforms) and Dr. W. Quiñones for anti-Hexokinase. Also special thanks to Rodrigo Vena for the assistance in the acquisition of the confocal microscopy images and Dolores Campos and Romina Manarin for their assistance in cell culture.

DECLARATION OF INTEREST

The authors declare no conflict of interest.

FUNDING INFORMATION

This work was supported by National Research Council (CONICET) grant PIP2010-0685 and National Agency of Scientific and Technological Promotion (ANPCyT) and Glaxo SmithKline joint grant PICTO2011- 0046.

AUTHOR CONTRIBUTION STATEMENT

Gabriela Vanina Villanova cloned and purified recombinant *Tc*BDF1 and raised the anti-*Tc*BDF1 antibodies in rabbit and mouse. Carla Ritagliati constructed the pTREX and p*Tc*INDEX-GW plasmids and transfected the parasites. Carla Ritagliati, Victoria Lucia Alonso and Pamela Cribb performed the western blot assays, immunofluorescence microscopies, growth curves and infection experiments. Carla Ritagliati and Gabriela Vanina Villanova performed the sequence alignments. Aline Araujo Zuma and María Cristina Machado Motta performed and interpreted the immunoelectron microscopies. Esteban Carlos Serra and Carla Ritagliati conceived and supervised the project, and wrote the article with contributions from all other authors.

REFERENCES

1. Kim SC, Sprung R, Chen Y, Xu Y, Ball H, Pei J, et al. Substrate and functional diversity of lysine acetylation revealed by a proteomics survey. Mol Cell. 2006 Aug;23(4):607-18.
2. Okanishi H, Kim K, Masui R, Kuramitsu S. Acetylome with structural mapping reveals the significance of lysine acetylation in Thermus thermophilus. J Proteome Res. 2013 Sep 6;12(9):3952-68.
3. Yu BJ, Kim JA, Moon JH, Ryu SE, Pan JG. The diversity of lysine-acetylated proteins in Escherichia coli. J Microbiol Biotechnol. 2008 Sep;18(9):1529-36.
4. Zhang J, Sprung R, Pei J, Tan X, Kim S, Zhu H, et al. Lysine acetylation is a highly abundant and evolutionarily conserved modification in Escherichia coli. Mol Cell Proteomics. 2009 Feb;8(2):215-25.

5. Wang Q, Zhang Y, Yang C, Xiong H, Lin Y, Yao J, et al. Acetylation of metabolic enzymes coordinates carbon source utilization and metabolic flux. Science. 2010 Feb 19;327(5968):1004-7.
6. Wu X, Vellaichamy A, Wang D, Zamdborg L, Kelleher NL, Huber SC, et al. Differential lysine acetylation profiles of Erwinia amylovora strains revealed by proteomics. J Proteomics. 2013 Feb 21;79:60-71.
7. Lee DW, Kim D, Lee YJ, Kim JA, Choi JY, Kang S, et al. Proteomic analysis of acetylation in thermophilic Geobacillus kaustophilus. Proteomics. 2013 Aug;13(15):2278-82.
8. Pan J, Ye Z, Cheng Z, Peng X, Wen L, Zhao F. Systematic analysis of the lysine acetylome in Vibrio parahemolyticus. J Proteome Res. 2014 Jul 3;13(7):3294-302.
9. Liu F, Yang M, Wang X, Yang S, Gu J, Zhou J, et al. Acetylome analysis reveals diverse functions of lysine acetylation in Mycobacterium tuberculosis. Mol Cell Proteomics. 2014 Dec;13(12):3352-66.
10. Mo R, Yang M, Chen Z, Cheng Z, Yi X, Li C, et al. Acetylome analysis reveals the involvement of lysine acetylation in photosynthesis and carbon metabolism in the model cyanobacterium Synechocystis sp. PCC 6803. J Proteome Res. 2015 Feb 6;14(2):1275-86.
11. Henriksen P, Wagner SA, Weinert BT, Sharma S, Bacinskaja G, Rehman M, et al. Proteome-wide analysis of lysine acetylation suggests its broad regulatory scope in Saccharomyces cerevisiae. Mol Cell Proteomics. 2012 Nov;11(11):1510-22.
12. Jeffers V, Sullivan WJ, Jr. Lysine Acetylation Is Widespread on Proteins of Diverse Function and Localization in the Protozoan Parasite Toxoplasma gondii. Eukaryot Cell. 2012 Jun;11(6):735-42.
13. Miao J, Lawrence M, Jeffers V, Zhao F, Parker D, Ge Y, et al. Extensive lysine acetylation occurs in evolutionarily conserved metabolic pathways and parasite-specific functions during Plasmodium falciparum intraerythrocytic development. Mol Microbiol. 2013 Aug;89(4):660-75.
14. Finkemeier I, Laxa M, Miguet L, Howden AJ, Sweetlove LJ. Proteins of diverse function and subcellular location are lysine acetylated in Arabidopsis. Plant Physiol. 2011 Apr;155(4):1779-90.
15. Weinert BT, Wagner SA, Horn H, Henriksen P, Liu WR, Olsen JV, et al. Proteome-wide mapping of the Drosophila acetylome demonstrates a high degree of conservation of lysine acetylation. Sci Signal. 2011;4(183):ra48.
16. Lundby A, Lage K, Weinert BT, Bekker-Jensen DB, Secher A, Skovgaard T, et al. Proteomic analysis of lysine acetylation sites in rat tissues reveals organ specificity and subcellular patterns. Cell Rep. 2012 Aug 30;2(2):419-31.
17. Choudhary C, Kumar C, Gnad F, Nielsen ML, Rehman M, Walther TC, et al. Lysine acetylation targets protein complexes and co-regulates major cellular functions. Science. 2009 Aug 14;325(5942):834-40.
18. Zhao S, Xu W, Jiang W, Yu W, Lin Y, Zhang T, et al. Regulation of cellular metabolism by protein lysine acetylation. Science. 2010 Feb 19;327(5968):1000-4.
19. Norvell A, McMahon SB. Cell biology. Rise of the rival. Science. 2010 Feb 19;327(5968):964-5.
20. Yang XJ. Lysine acetylation and the bromodomain: a new partnership for signaling. Bioessays. 2004 Oct;26(10):1076-87.
21. Villanova GV, Nardelli SC, Cribb P, Magdaleno A, Silber AM, Motta MC, et al. Trypanosoma cruzi bromodomain factor 2 (BDF2) binds to acetylated histones and is accumulated after UV irradiation. Int J Parasitol. 2009 May;39(6):665-73.
22. Alonso VL, Villanova GV, Ritagliati C, Machado Motta MC, Cribb P, Serra EC. Trypanosoma cruzi bromodomain factor 3 binds acetylated alpha-tubulin and concentrates in the flagellum during metacyclogenesis. Eukaryot Cell. 2014 Jun;13(6):822-31.
23. Opperdoes FR. Compartmentation of carbohydrate metabolism in trypanosomes. Annu Rev Microbiol. 1987;41:127-51.

24. Michels PA, Hannaert V, Bringaud F. Metabolic aspects of glycosomes in trypanosomatidae - new data and views. Parasitol Today. 2000 Nov;16(11):482-9.
25. Wiemer EA, L IJ, van Roy J, Wanders RJ, Opperdoes FR. Identification of 2-enoyl coenzyme A hydratase and NADP(+)-dependent 3-hydroxyacyl-CoA dehydrogenase activity in glycosomes of procyclic Trypanosoma brucei. Mol Biochem Parasitol. 1996 Nov 12;82(1):107-11.
26. Concepcion JL, Gonzalez-Pacanowska D, Urbina JA. 3-Hydroxy-3-methyl-glutaryl-CoA reductase in Trypanosoma (Schizotrypanum) cruzi: subcellular localization and kinetic properties. Arch Biochem Biophys. 1998 Apr 1;352(1):114-20.
27. Urbina JA, Concepcion JL, Rangel S, Visbal G, Lira R. Squalene synthase as a chemotherapeutic target in Trypanosoma cruzi and Leishmania mexicana. Mol Biochem Parasitol. 2002 Nov-Dec;125(1-2):35-45.
28. Opperdoes FR, Szikora JP. In silico prediction of the glycosomal enzymes of Leishmania major and trypanosomes. Mol Biochem Parasitol. 2006 Jun;147(2):193-206.
29. Galland N, de Walque S, Voncken FG, Verlinde CL, Michels PA. An internal sequence targets Trypanosoma brucei triosephosphate isomerase to glycosomes. Mol Biochem Parasitol. 2010 May;171(1):45-9.
30. Bouvier LA, Camara Mde L, Canepa GE, Miranda MR, Pereira CA. Plasmid vectors and molecular building blocks for the development of genetic manipulation tools for Trypanosoma cruzi. PLoS One. 2013;8(10):e80217.
31. Hendriksen CF. Introduction: laboratory animals and immunization procedures: challenges and opportunities. ILAR J. 2005;46(3):227-9.
32. Contreras VT, Araujo-Jorge TC, Bonaldo MC, Thomaz N, Barbosa HS, Meirelles Mde N, et al. Biological aspects of the Dm 28c clone of Trypanosoma cruzi after metacyclogenesis in chemically defined media. Mem Inst Oswaldo Cruz. 1988 Jan-Mar;83(1):123-33.
33. Rasband WS. ImageJ software. In: U. S. National Institutes of Health B, Maryland, USA, editor. http://imagejnihgov/ij/1997-2011.
34. Ferreira LR, Dossin Fde M, Ramos TC, Freymuller E, Schenkman S. Active transcription and ultrastructural changes during Trypanosoma cruzi metacyclogenesis. An Acad Bras Cienc. 2008 Mar;80(1):157-66.
35. Opperdoes FR. Miconazole: an inhibitor of cyanide-insensitive respiration in Trypanosoma brucei. Trans R Soc Trop Med Hyg. 1980;74(3):423-4.
36. Zeng L, Zhou MM. Bromodomain: an acetyl-lysine binding domain. FEBS Lett. 2002 Feb 20;513(1):124-8.
37. Roy A, Kucukural A, Zhang Y. I-TASSER: a unified platform for automated protein structure and function prediction. Nat Protoc. 2010 Apr;5(4):725-38.
38. Milagros Camara Mde L, Bouvier LA, Miranda MR, Pereira CA. Identification and validation of Trypanosoma cruzi's glycosomal adenylate kinase containing a peroxisomal targeting signal. Exp Parasitol. 2012 Apr;130(4):408-11.
39. Swinkels BW, Gould SJ, Bodnar AG, Rachubinski RA, Subramani S. A novel, cleavable peroxisomal targeting signal at the amino-terminus of the rat 3-ketoacyl-CoA thiolase. EMBO J. 1991 Nov;10(11):3255-62.
40. Blattner J, Dorsam H, Clatyon CE. Function of N-terminal import signals in trypanosome microbodies. FEBS Lett. 1995 Mar 6;360(3):310-4.
41. Dhalluin C, Carlson JE, Zeng L, He C, Aggarwal AK, Zhou MM. Structure and ligand of a histone acetyltransferase bromodomain. Nature. 1999 Jun 3;399(6735):491-6.

42. Alonso VL, Ritagliati C, Cribb P, Serra EC. Construction of three new Gateway(R) expression plasmids for Trypanosoma cruzi. Mem Inst Oswaldo Cruz. 2014 Nov 21;0:0.
43. Elias MC, da Cunha JP, de Faria FP, Mortara RA, Freymuller E, Schenkman S. Morphological events during the Trypanosoma cruzi cell cycle. Protist. 2007 Apr;158(2):147-57.
44. Crowley T, Brunori M, Rhee K, Wang X, Wolgemuth DJ. Change in nuclear-cytoplasmic localization of a double-bromodomain protein during proliferation and differentiation of mouse spinal cord and dorsal root ganglia. Brain Res Dev Brain Res. 2004 Apr 19;149(2):93-101.
45. Crowley TE, Kaine EM, Yoshida M, Nandi A, Wolgemuth DJ. Reproductive cycle regulation of nuclear import, euchromatic localization, and association with components of Pol II mediator of a mammalian double-bromodomain protein. Mol Endocrinol. 2002 Aug;16(8):1727-37.
46. Trousdale RK, Wolgemuth DJ. Bromodomain containing 2 (Brd2) is expressed in distinct patterns during ovarian folliculogenesis independent of FSH or GDF9 action. Mol Reprod Dev. 2004 Jul;68(3):261-8.
47. Ritagliati C, Alonso VL, Manarin R, Cribb P, Serra EC. Overexpression of cytoplasmic TcSIR2RP1 and mitochondrial TcSIR2RP3 impacts on Trypanosoma cruzi growth and cell invasion. PLoS Negl Trop Dis. 2015 Apr;9(4):e0003725.
48. Haanstra JR, Gonzalez-Marcano EB, Gualdron-Lopez M, Michels PA. Biogenesis, maintenance and dynamics of glycosomes in trypanosomatid parasites. Biochim Biophys Acta. 2015 Sep 16.
49. Szoor B, Haanstra JR, Gualdron-Lopez M, Michels PA. Evolution, dynamics and specialized functions of glycosomes in metabolism and development of trypanosomatids. Curr Opin Microbiol. 2014 Dec;22:79-87.
50. Jiang W, Wang S, Xiao M, Lin Y, Zhou L, Lei Q, et al. Acetylation regulates gluconeogenesis by promoting PEPCK1 degradation via recruiting the UBR5 ubiquitin ligase. Mol Cell. 2011 Jul 8;43(1):33-44.
51. Lux H, Heise N, Klenner T, Hart D, Opperdoes FR. Ether--lipid (alkyl-phospholipid) metabolism and the mechanism of action of ether--lipid analogues in Leishmania. Mol Biochem Parasitol. 2000 Nov;111(1):1-14.
52. Richmond GS, Gibellini F, Young SA, Major L, Denton H, Lilley A, et al. Lipidomic analysis of bloodstream and procyclic form Trypanosoma brucei. Parasitology. 2010 Aug;137(9):1357-92.
53. Eglen RM, Reisine T. Screening for compounds that modulate epigenetic regulation of the transcriptome: an overview. J Biomol Screen. 2011 Dec;16(10):1137-52.
54. Zheng W. Sirtuins as emerging anti-parasitic targets. Eur J Med Chem. 2013 Jan;59:132-40.
55. Wang CY, Filippakopoulos P. Beating the odds: BETs in disease. Trends Biochem Sci. 2015 Aug;40(8):468-79.
56. Sanchez R, Meslamani J, Zhou MM. The bromodomain: from epigenome reader to druggable target. Biochim Biophys Acta. 2014 Aug;1839(8):676-85.

Figure Legends.

Figure 1. The expression of *Tc*BDF1 is developmentally regulated. Equal amounts of CL Brener total lysates (TL) from epimastigotes (E), amastigotes (A) and trypomastigotes (T) were loaded on SDS-PAGE and transferred to nitrocellulose membrane. (A) Ponceau S staining and western blot analysis using the following antibodies: a-*Tc*BDF1 and a-Tubulin α as load control. The degree of expression observed were quantified and normalized to α-tubulin intensity. (B) Immunofluorescence assay of CL Brener wild type epimastigotes, amastigotes and

trypomastigotes using a-*Tc*BDF1. FITC-conjugated anti-rabbit (green) was used as secondary antibody and DNA was stained with DAPI (blue). Scale bar: 5 μm.

Figure 2. Subcellular fractionations. (A) Equal amounts of Nuclear (N) and Non-Nuclear (NoN) extracts were loaded on SDS-PAGE and Coomassie stained (left panel) or transferred to a nitrocellulose membrane and assayed with: a-*Tc*BDF1, a-*Tc*BDF2 (nuclear marker) and a-*Tc*TAT (cytosolic marker). (B) Western blot analysis of the subcellular fractions obtained by differential centrifugation. The fractions were loaded on SDS-PAGE (left panel) followed by western blot with a-*Tc*BDF1, a-*Tc*BDF2, a-*Tc*MDHm (mitochondrial), a-*Tc*MDHg, a-*Tc*HK (glycosomal) and a-*Tc*TAT. N, nucleus; LG, large granules; SG, small granules; M, microsomes; S, final supernatant. (C) Digitonin fractionation. The fractions were loaded on SDS-PAGE (upper panel) followed by western blot with a-*Tc*BDF1, a-*Tc*MDHm, a-*Tc*MDHg, a-*Tc*HK, a-*Tc*BDF3 (cytosolic) and a-*Tc*TAT.

Figure 3. *Tc*BDF1 localizes in the glycosomes. (A) Immunofluorescence assay of CL Brener wild type epimastigotes using rabbit antibodies against *Tc*HK and mouse antibodies against *Tc*BDF1. Cy3-conjugated anti-rabbit (red) and FITC-conjugated anti-mouse (green) were used as secondary antibodies. (B) Confocal microscopy analysis of transient epimastigotes co-transfected with pTEX-GFP-PTS1 and pTREX-*Tc*BDF1-Cherry. DNA was counterstained with DAPI (blue). Scale bar: 5 μm.

Figure 4. *Tc*BDF1 is directed to the glycosomes by its N-terminal PTS2 signal. Confocal microscopy analysis of transient epimastigotes transfected with the following constructs: pTREX-*Tc*BDF1-Cherry, pTREX-*Tc*BDF1ΔN-Cherry or pTREX-PTS2-Cherry. DNA was counterstained with DAPI (blue). Scale bar: 5 μm.

Figure 5. Inducible expression of *Tc*BDF1wtHA and *Tc*BDF1dmHA. Equal amounts of parasite total lysate (TL) from each line in the absence (-) or presence (+) of 0.5 μg/ml Tetracycline for 24 hours, were loaded on SDS-PAGE and stained with Coomassie (left panel), followed by western blot analysis using rat a-HA monoclonal antibodies (A), or rabbit polyclonal antibodies against *Tc*BDF1 and mouse a-Tubulin α as load control. (B) The degree of overexpression observed with the specific antibodies were quantified and normalized to α-tubulin intensity. (C) Immunofluorescence microscopy of uninduced and induced (0.5 μg/ml Tetracycline, 24 hours) parasites using rat anti-HA and FITC-conjugated anti-rat antibodies (green). DNA was stained with DAPI (blue). Images obtained with a Nikon Ni-U microscope.

Figure 6. Overexpression of *Tc*BDF1wtHA is deleterious for epimastigotes. (A) Growth curves of epimastigotes transfected with p*Tc*INDEXGW-BDF1wtHA and BDF1dmHA in the absence (closed circles, grey line) or presence (closed squares, black line) of 0.5 μg/ml Tetracycline (which was re-added every 5 days) counted daily during 10 days. Results are representative of three independent experiments. (B) Giemsa stained p*Tc*INDEXGW-BDF1wtHA epimastigotes in the absence (- Tet) or presence of Tetracycline (+ Tet). Images obtained with a Nikon Ni-U microscope.

Figure 7. Overexpression of *Tc*BDF1wtHA triggers apoptosis. Electron microscopy analysis of the ultrastructure of the p*Tc*INDEXGW-BDF1wtHA cell line in the absence (A and G) or presence (B-I) of Tetracycline. The nucleolus region, which probably corresponds to the granular domain, is seen condensed (B, arrow) and fragmented (C, arrows). In induced cells the nucleolus is completely fragmented (D, arrows) and the nuclear structure is completely disorganized (E).

Chromatin compactation (F, arrow) is observed near the nuclear envelope, this indicates apoptosis. Note also the cytoplasm extraction in induced *Tc*BDF1wtHA cells (F). Non induced parasites (G) presented glycosomes (g) with their typical ultrastructure. Induced cells (H-I) presented larger glycosomes with lower electrodensity. Nu = nucleolus; ht = heterochromatin; K= kinetoplast. Bars: (A) 0,5 μM; (B - E) 1 μM; (F) 2 μM. (G - H) = 1 μM; (I) and inset = 0,5 μM.

Figure 8. Effect of the overexpression of wild type and mutant *Tc*BDF1 on *in vitro* metacyclogenesis. *In vitro* metacyclogenesis using TAU medium of lines harboring transgenes encoding *Tc*BDF1wtHA and *Tc*BDF1dmHA uninduced (- Tet) or induced (+ Tet) with 0.5 μg/ml Tetracycline. The bar graph represents the mean ± SEM from three independent experiments; ** $P<0.005$ (unpaired, two-tailed Student t test).

Figure 9. *Tc*BDF1 overexpression impacts on Vero cells infection. The infection and the post-infection incubation were performed in the absence or presence of 0.25 μg/ml Tetracycline: (-/-), Tet was never added to the medium; (+/-), trypomastigotes were pre-treated with Tet for 3 hours prior to infection, and it was added during the infection but not after; (-/+), trypomastigotes were not induced, Tet was only added for 72 hours post-infection at the amastigote stage; (+/+), trypomastigotes were pre-treated and Tet was present at all times. The percentage of infected cells (A) and the number of amastigotes per cell (B) were determined by counting Giemsa-stained slides using a light microscope. Results are expressed as means ± SEM of triplicates, and represent one of three independent experiments performed. Each condition was analyzed by unpaired Mann-Whitney two-tailed Student t test with the control (-/-): * $P<0.05$, ** $P<0.005$, *** $P<0.001$, **** $P<0.0001$.

Supplemental Figure Legends

S1 Figure. *Tc*BDF1 sequence alignment and modeling. (A) Alignment of *Tc*BDF1 with its orthologs from *T. brucei* and *L. major* and with the two characterized bromodomain-containing proteins from *T. cruzi* (*Tc*BDF2 and *Tc*BDF3), together with the secondary structure prediction (on top). (B) Sequence alignment of a selected number of bromodomains of different organisms. The sequences used were: *Dm*Brahma (Drosophila *melanogaster;* P25439), *Hs*SMCA4 (Homo *sapiens;* P51532), *Hs*SMCA2 (H. *sapiens;* P51531), *Dm*GCN*5* (D. *melanogaster;* AAC39102.1), *Hs*GCN5 (H. *sapiens;* AAC39769.1), *Sc*Gcn5p (Saccharomyces *cerevisiae;* NP_011768.1), *Sc*BDF1a and *Sc*BDF1b (S. *cerevisiae;* P35817), *Sc*BDF2a and *Sc*BDF2b (S. *cerevisiae;* YDL070W), *Dm*TAF1a (TAFII250) and *Dm*TAF1b (TAFII250) (D.melanogaster; P51123), *Hs*TAF1a (TAFII250) and *Hs*TAF1b (TAFII250) (H. *sapiens;* P21675), *Sc*Spt7 (S. *cerevisiae;* NP_009637.1), *Af*Spt7 (Aspergillus *fumigatus;* XP_754519.1), *Tc*BDF1 (T. *cruzi;* TcCLB.506247.80). Both alignments were performed using ClustalX2.1 and edited with the ESPript server (http://espript.ibcp.fr/ESPript/ESPript). The bromodomain α-helixes are squared in blue. Identical residues are white shaded in red and conservative changes in red shaded in white. Asterisks show residues important for the interaction with the acetylated lysine. (C) Three-dimensional structure for *Tc*BDF1 predicted by I-TASSER. The residues important for the interaction with the acetylated lysine are labelled.

S2 Figure. Alignment of multiple PTS2 sequences from different organisms using ClustalX2.1 and edited to highlight conserved (black, shaded grey) and identical (white, shaded black) amino acid residues. The nonapeptide is squared in blue. DHAP, dihydroxyacetone phosphate; MDH, malate

dehydrogenase; HK, hexokinase; PEX11, peroxisome receptor; GAPDH, gyceraldehyde 3-phosphate dehydrogenase; CP, carboxypeptidase.

S3 Figure. Alignment of *Tc*BDF1 and human PCAF bromodomains using ClustalX2.1 and manually edited to highlight conserved (bold, white background) and identical (black background) residues based on BLOSUM 62 substitution matrix data. Alpha helixes are squared. Asterisks show residues important for the interaction with the acetylated lysine, and the mutated amino acids are depicted with arrows.

Fig 1

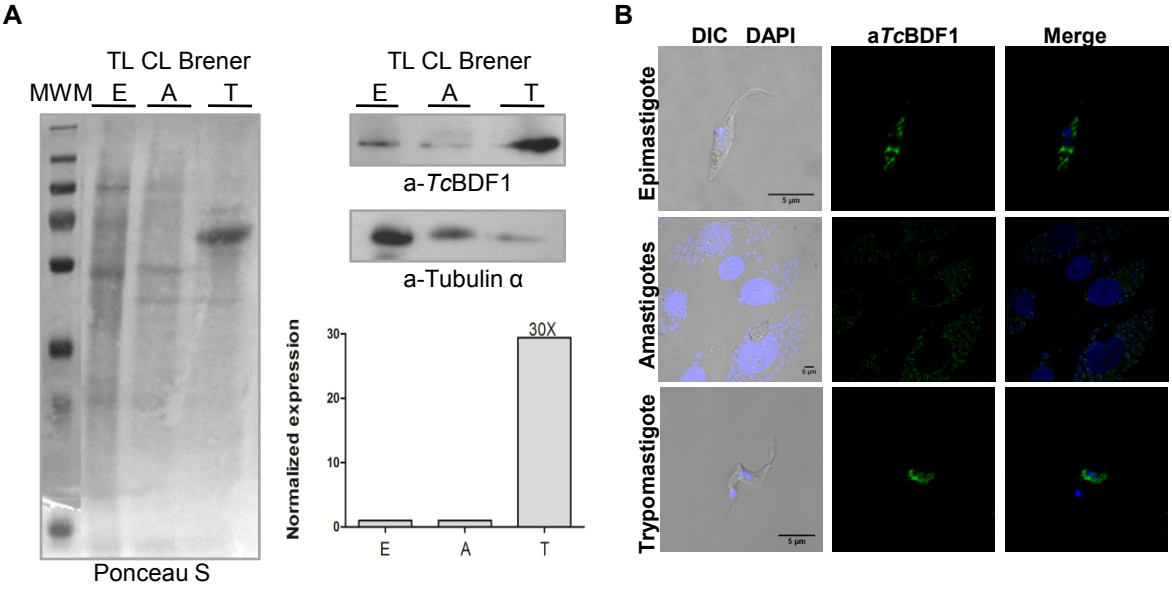
A
TL CL Brener
MWM E A T
Ponceau S
TL CL Brener
E A T
a-*Tc*BDF1
a-Tubulin α
Normalized expression
30X
30
20
10
0
E
A
T
B
DIC DAPI
a*Tc*BDF1
Merge
Epimastigote
Amastigotes
Trypomastigote

Fig 2

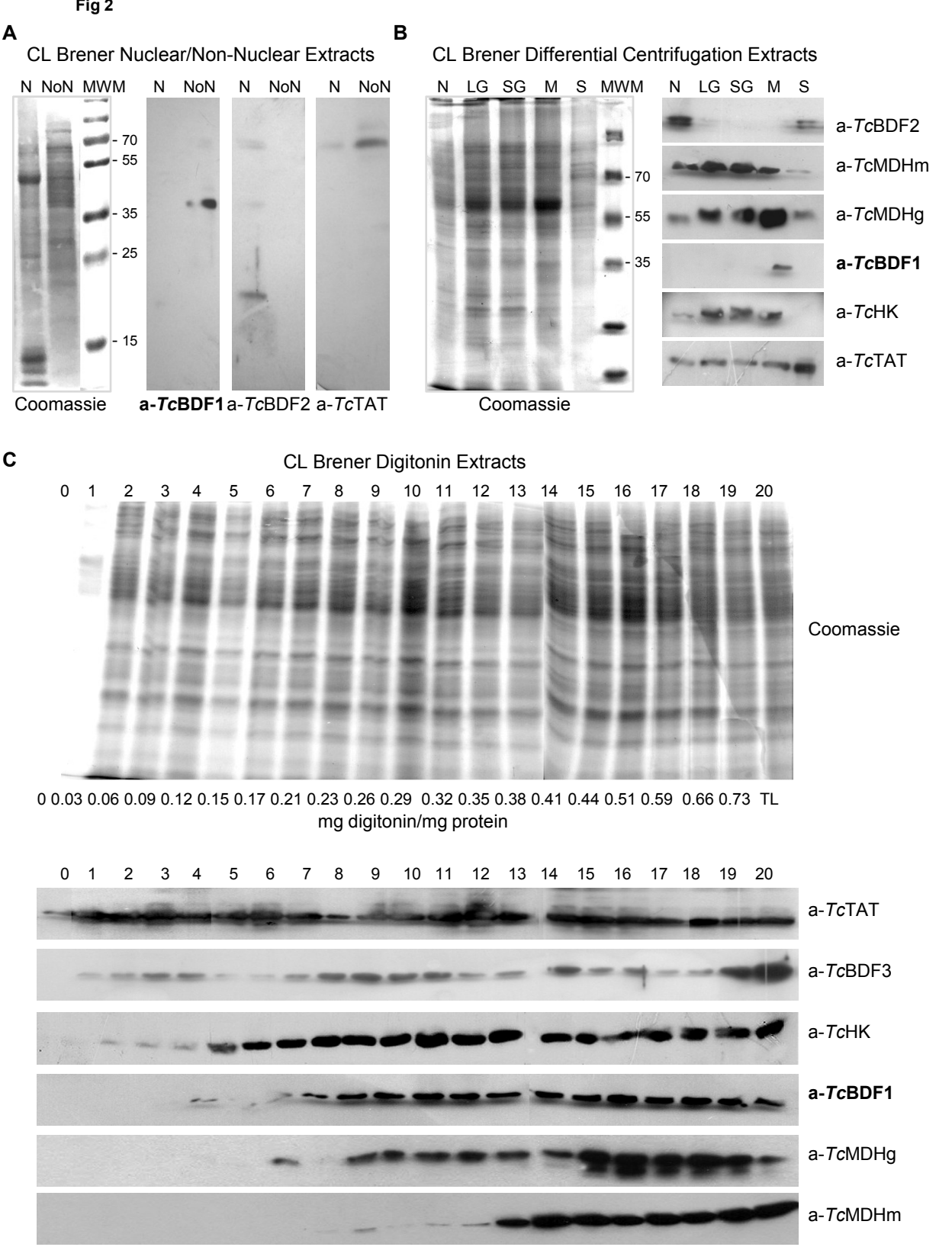
A
CL Brener Nuclear/Non-Nuclear Extracts
N NoN MWM N NoN N NoN N NoN
70
55
35
25
15
Coomassie
a-TcBDF1 a-TcBDF2 a-TcTAT
B
CL Brener Differential Centrifugation Extracts
N LG SG M S MWM N LG SG M S
70
55
35
Coomassie
a-TcBDF2
a-TcMDHm
a-TcMDHg
a-TcBDF1
a-TcHK
a-TcTAT
C
CL Brener Digitonin Extracts
0 1 2 3 4 5 6 7 8 9 10 11 12 13 14 15 16 17 18 19 20
Coomassie
0 0.03 0.06 0.09 0.12 0.15 0.17 0.21 0.23 0.26 0.29 0.32 0.35 0.38 0.41 0.44 0.51 0.59 0.66 0.73 TL
mg digitonin/mg protein
0 1 2 3 4 5 6 7 8 9 10 11 12 13 14 15 16 17 18 19 20
a-TcTAT
a-TcBDF3
a-TcHK
a-TcBDF1
a-TcMDHg
a-TcMDHm

Fig 3

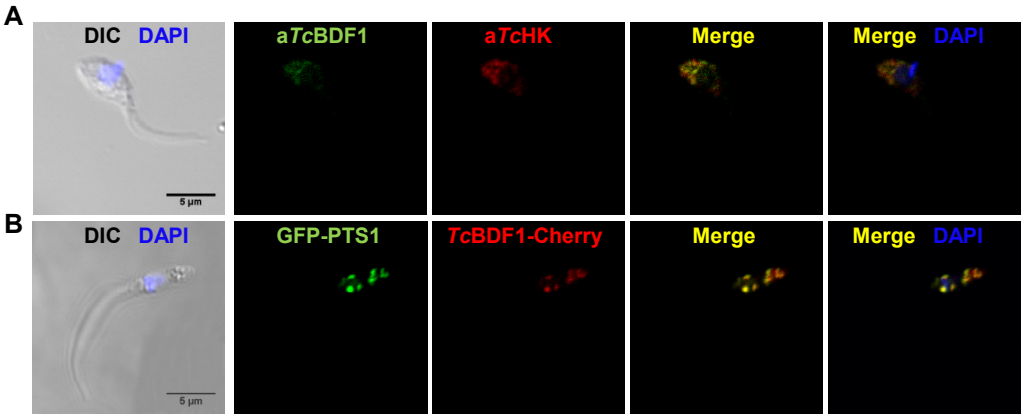
A
DIC DAPI
a*Tc*BDF1
a*Tc*HK
Merge
Merge DAPI
5 µm
B
DIC DAPI
GFP-PTS1
*Tc*BDF1-Cherry
Merge
Merge DAPI
5 µm

Fig 4

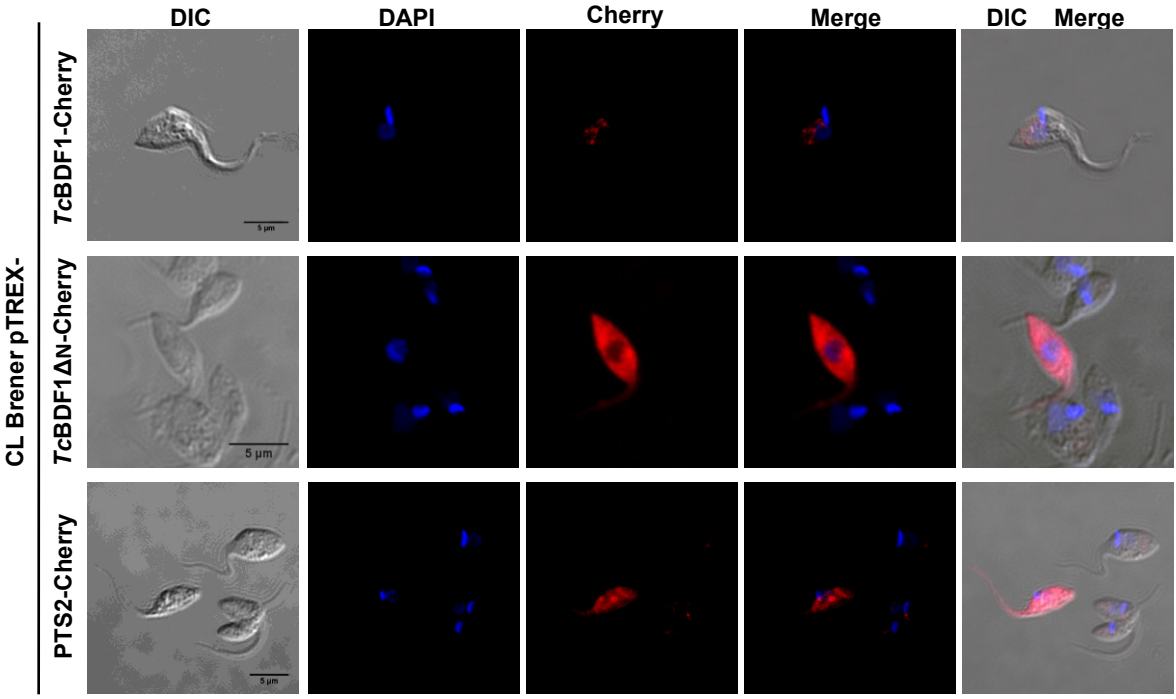
DIC
DAPI
Cherry
Merge
DIC Merge
CL Brener pTREX-
TcBDF1-Cherry
TcBDF1ΔN-Cherry
PTS2-Cherry
5 µm

Fig 5

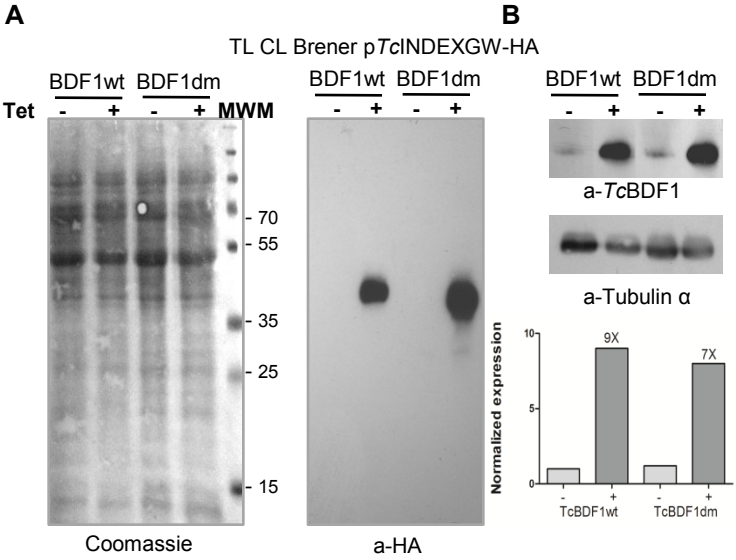
A
TL CL Brener pTcINDEXGW-HA
BDF1wt BDF1dm BDF1wt BDF1dm
Tet - + - + MWM - + - +
70
55
35
25
15
Coomassie
a-HA
B
BDF1wt BDF1dm
- + - +
a-TcBDF1
a-Tubulin α
Normalized expression
9X
7X
10
5
0
TcBDF1wt
TcBDF1dm

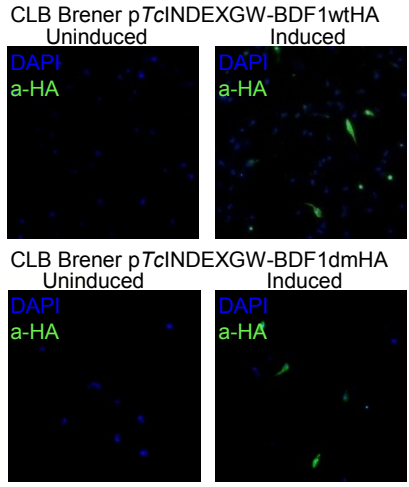
C
CLB Brener pTcINDEXGW-BDF1wtHA
Uninduced
Induced
DAPI
a-HA
CLB Brener pTcINDEXGW-BDF1dmHA
Uninduced
Induced
DAPI
a-HA

Fig 6

A

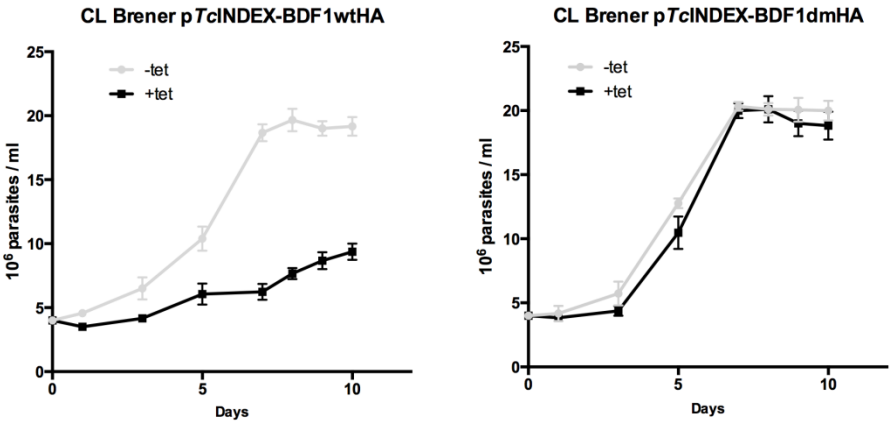
CL Brener pTcINDEX-BDF1wtHA
-tet
+tet
10^6 parasites / ml
Days
CL Brener pTcINDEX-BDF1dmHA
-tet
+tet
10^6 parasites / ml
Days

B

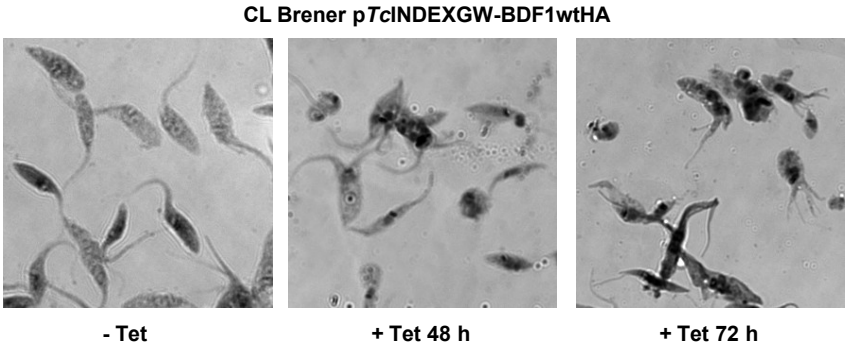
CL Brener pTcINDEXGW-BDF1wtHA
- Tet
+ Tet 48 h
+ Tet 72 h

Fig 7

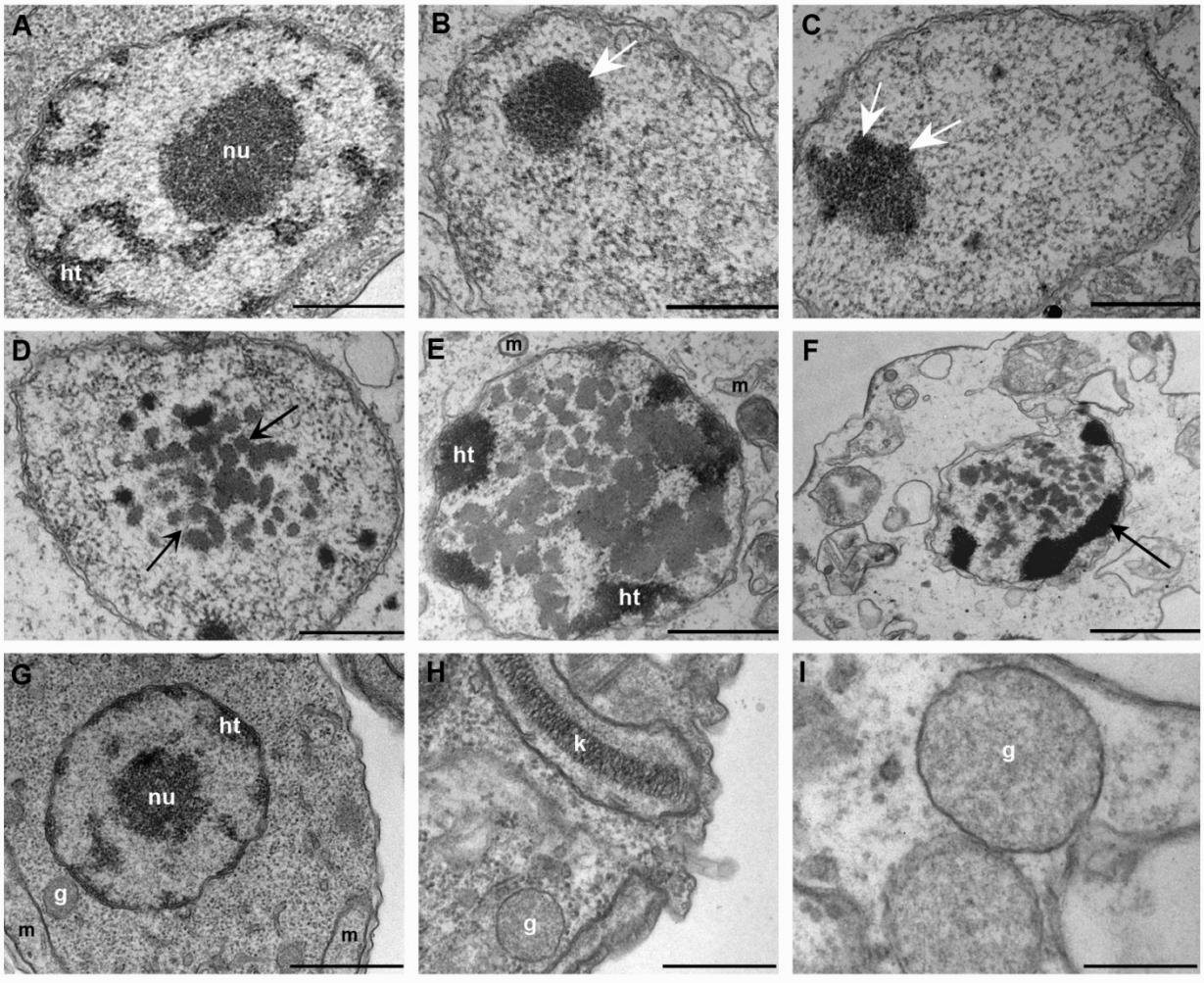

Fig 8

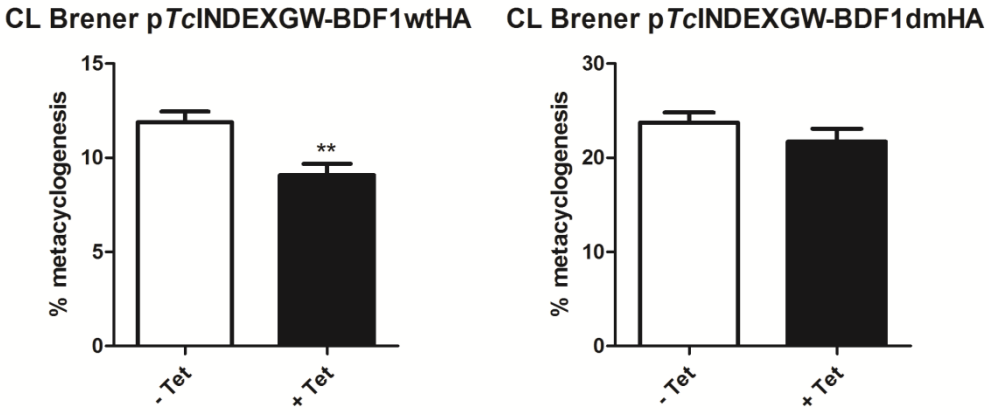
CL Brener pTcINDEXGW-BDF1wtHA
% metacyclogenesis
15
10
5
0
**
- Tet
+ Tet
CL Brener pTcINDEXGW-BDF1dmHA
% metacyclogenesis
30
20
10
0
- Tet
+ Tet

Fig 9

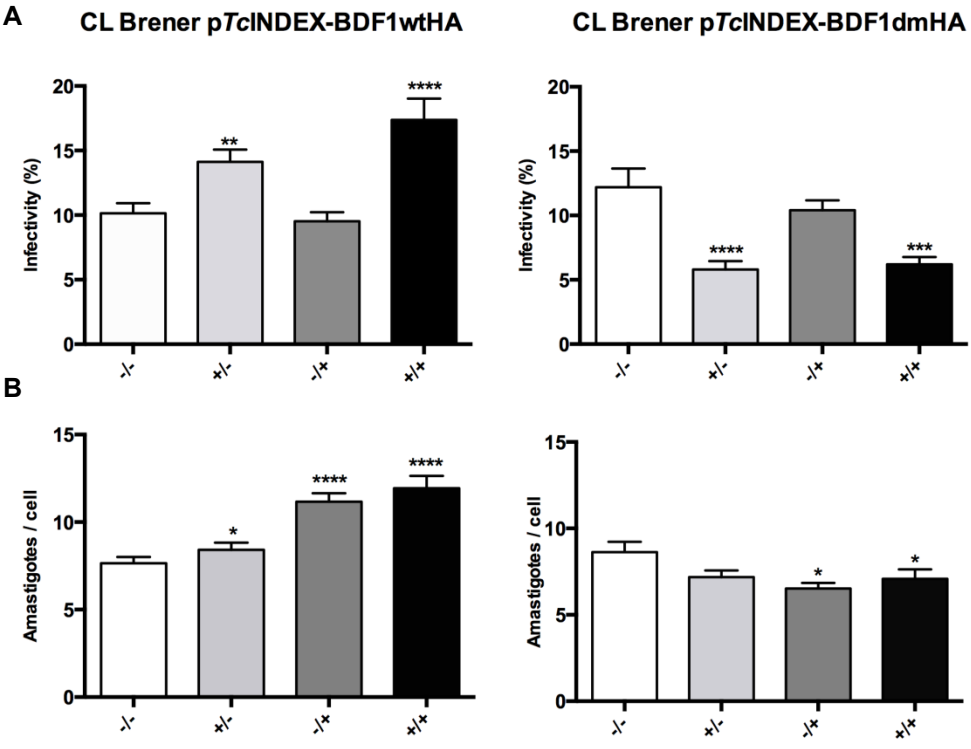
A
CL Brener pTcINDEX-BDF1wtHA
CL Brener pTcINDEX-BDF1dmHA
Infectivity (%)
20
15
10
5
0
**
****
****
***
-/-
+/-
-/+
+/+
B
Amastigotes / cell
15
10
5
0
*
****
****
*
*
-/-
+/-
-/+
+/+